INTERNATIONAL JOURNAL FOR NUMERICAL METHODS IN ENGINEERING
Int. J. Numer. Meth. Engng 2001; **51**:1385–1405 (DOI: 10.1002/nme.181)

Die shape design optimization of sheet metal stamping process using meshfree method

Nam Ho Kim[†,‡], Kyung Kook Choi[*,§,¶] and Jiun Shyan Chen[‖,**]

Center for Computer-Aided Design and Department of Mechanical Engineering, College of Engineering, The University of Iowa, Iowa City, IA 52242, U.S.A.

SUMMARY

A die shape design sensitivity analysis (DSA) and optimization for a sheet metal stamping process is proposed based on a Lagrangian formulation. A hyperelasticity-based elastoplastic material model is used for the constitutive relation that includes a large deformation effect. The contact condition between a workpiece and a rigid die is imposed through the penalty method with a modified Coulomb friction model. The domain of the workpiece is discretized by a meshfree method. A continuum-based DSA with respect to the rigid die shape parameter is formulated using a design velocity concept. The die shape perturbation has an effect on structural performance through the contact variational form. The effect of the deformation-dependent pressure load to the design sensitivity is discussed. It is shown that the design sensitivity equation uses the same tangent stiffness matrix as the response analysis. The linear design sensitivity equation is solved at each converged load step without the need of iteration, which is quite efficient in computation. The accuracy of sensitivity information is compared to that of the finite difference method with an excellent agreement. A die shape design optimization problem is solved to obtain the desired shape of the workpiece to minimize spring-back effect and to show the feasibility of the proposed method. Copyright © 2001 John Wiley & Sons, Ltd.

KEY WORDS: design sensitivity analysis; design optimization; elastoplasticity; sheet metal stamping

1. INTRODUCTION

The theory of shape design sensitivity analysis (DSA) through the perturbation of a continuum [1] is well established where the structural domain is concerned as a design. However, in the

*Correspondence to: K. K. Choi, Center for Computer-Aided Design and Department of Mechanical Engineering, College of Engineering, University of Iowa, 208 Engineering Research Facility, Iowa City, IA 52242-1000, U.S.A.
†Postdoctoral Associate
‡E-mail: nkim@ccad.uiowa.edu
§Director and Professor
¶E-mail: kkchoi@ccad.uiowa.edu
‖Associate Professor
**E-mail: jschen@icaen.uiowa.edu

Contract/grant sponsor: NSF/DARPA OPAAL; contract/grant number: DMS98-74015
Contract/grant sponsor: Ford University Research Program; contract/grant number: URP 97-723R

Received 21 October 1999
Revised 1 June 2000

sheet metal stamping process, the shape of the workpiece is usually not a design and the quality of the product depends on the die shape design. In this paper, the dependence of the structural performance on the shape of the rigid die is investigated to improve the quality of the product through design optimization. Since the geometry of the workpiece is fixed, this problem is classified as a sizing DSA compared to the shape DSA where the geometry of structure is a design parameter. However, the design velocity concept of the shape DSA is adopted here to describe the perturbation of the die shape.

The response analysis of the manufacturing process can be carried out using the flow formulation or Lagrangian formulation. The flow formulation ignores the elastic deformation and follows the process similar to non-Newtonian fluid analysis [2]. However, lack of ability in computing the residual stress and the spring-back phenomenon at the end of the process is a major disadvantage in spite of the simplicity of the formulation. Several research results are reported for DSA using the rigid plastic material model. Maniatty and Chen [3] developed a design sensitivity formulation for the steady-state metal-forming process using a semi-analytical adjoint variable method. Antunez and Kleiber [4] proposed a shape DSA for a steady-state forming process using a control volume method. Zhao *et al.* [5] solved an unconstrained optimization problem to minimize the difference between the shape of the stamped workpiece and the desired shape. Their sensitivity equation requires an additional tangent stiffness matrix that is different from the one in response analysis. Chung and Hwang [6] proposed a method for transient forming process optimization. Since a semi-analytical method is used to compute sensitivity coefficient, the accuracy depends on the size of design perturbation. Balagangadhar and Tortorelli [7] discussed design optimization of steady-state manufacturing processes using a reference frame approach. The shape DSA procedure for steady-state is similar to that of linear elasticity and the adjoint variable method is applicable. For shape DSA of large deformation problems, since the shape design parameters are defined at the undeformed geometry and the analysis configuration is updated at each time step for the transient forming process, an appropriate transformation to the undeformed configuration or design velocity updating procedure has to be considered. No research result has been presented to address this issue, and many shape sensitivity results for a transient forming process are not quite accurate.

The Lagrangian formulation is a computationally demanding procedure compared to the flow formulation. However, accurate computations of the spring-back phenomena and the residual stress at the end of the process are advantages offered by the Lagrangian formulation. The matured development of the elastoplasticity theory for large deformation significantly enhances solution accuracy in the simulation of the sheet metal stamping process. The multiplicative decomposition of the deformation gradient into elastic and plastic parts is proposed by Lee [8] through defining a stress-free intermediate configuration and using a hyperelastic constitutive relation for elastic deformation. This constitutive model is preferred for numerical solution of large deformation in isotropic material. This model is well suited for the single-crystal metal plasticity. A computational framework of this theory is developed by Simo [9], which preserves the conventional return mapping algorithm in the principal stress space. For a detailed discussion of finite deformation elastoplasticity with multiplicative decomposition, refer to References [9–13].

A Lagrangian formulation of DSA for the multiplicative elastoplasticity is developed by Badrinarayanan and Zabaras [14] for die shape and process design. They pointed out that the tangent stiffness matrix of the response analysis is different from that of the design sensitivity

equation. The tangent stiffness matrix is computed again for DSA, and this procedure reduces computational efficiency. It should be noted that if the linearization is consistently developed, then the sensitivity equation has to contain the same tangent stiffness matrix as response analysis. Recently, Wiechmann and Barthold [15] derived sensitivity formulation using the same tangent stiffness matrix as response analysis through consistent linearization. In this paper, a Lagrangian formulation of sizing DSA is developed, and the same tangent stiffness as response analysis is used in DSA without iteration.

Mathematically, a contact problem can be formulated as a variational inequality where the solution in the Hilbert space is projected onto the constraint set. This constrained optimization problem can be approximated using the Lagrange multiplier method or penalty method. A frictional contact condition can be formulated using the penalty method and a modified Coulomb friction law. In literature, the directional differentiability of the projected solution onto the constraint set was proven for linear problems [16]. The design sensitivity of the solution of the contact problem, which is the solution of another variational inequality, can be approximated by taking a design derivative of the approximated minimization problem. It can be shown that the approximate design sensitivity of the solution of the contact problem converges to the solution of the variational inequality for linear problems. With a lack of mathematical proof of the existence of the design sensitivity for non-linear problems, the design derivative of the approximated penalty method is taken for the finite deformation frictional contact problem [17, 18]. It was shown that path dependency comes from the frictional effects, whereas the normal contact condition is path independent. The shape change of the rigid die is considered for DSA in this paper. The structural response depends on the shape change of the rigid surface through the contact variational form.

A pressure-dependent boundary condition is of particular interest in a finite deformation problem. As the structure experiences deformation, the direction of the surface traction changes. The integration of the surface traction through the boundary is transformed to a parametric space. The residual force is computed based on the current configuration and the tangent stiffness becomes non-symmetric. Detailed formulations of the boundary pressure load within the context of the finite element method are discussed by Hibbitt [19]; Schweizerhof and Ramm [20]; and by Simo *et al.* [21] for axi-symmetric problems. The design sensitivity formulation of the boundary pressure load can be described in the context of parametric representation. Since the perturbation of the design does not affect the parametric space, the design differentiation can operate directly on the parametric integration without complication. It turns out that the fictitious load term corresponding to the boundary pressure load explicitly depends only on design at the undeformed configuration, which means that the sensitivity equation is path independent even if the load is non-conservative.

In general, the sheet metal experiences large deformation during the stamping process. An effective numerical method that can handle mesh distortion problems in the conventional finite element method is highly desirable in analysing finite deformation problems. Recently, researchers have focused on numerical methods that discretize a domain without using meshes to alleviate these difficulties. A number of meshfree methods that do not require explicit meshes in domain discretization have been proposed. Belytschko *et al.* [22, 23] proposed the element-free Galerkin (EFG) method that solves structural problem accurately and uses the Lagrange multiplier method to impose the essential boundary conditions. Liu *et al.* [24] developed the reproducing kernel particle method (RKPM) by introducing a modified kernel function that is constructed by enforcing the reproducing conditions so that the kernel estimate

of the displacement exactly reproduces polynomials up to a certain degree. The RKPM was further extended to highly non-linear hyperelastic, elastoplastic, and contact problems by Chen *et al.* [25, 26] The meshfree method is an ideal choice for the metal stamping process since, unlike the conventional finite element method, the solution is not sensitive to mesh distortion. The RKPM is utilized in this paper for response analysis of the metal stamping process and, thus, DSA. However, the design sensitivity formulation presented in this paper is based on a continuum approach, and therefore all the equations are applicable to other methods, such as the finite element method, if appropriate discretization is used.

The outline of the paper is as follows. After introduction and the literature review in Section 1, sizing DSA for a structural problem including a large deformation elastoplasticity is introduced in Section 2 with the multiplicative decomposition formulation. In Section 3, a die shape DSA is formulated by taking the derivative of the contact constraint with respect to the die shape and this is then combined with a structural equation derived in Section 2 to establish the sensitivity equation. For the application to the pressurized stamping process, the contributions of the pressure load to the response analysis and DSA are investigated in Section 4. To demonstrate the accuracy and efficiency of the proposed approach, die shape design optimization of the sheet metal stamping process is shown in Section 5.

2. DESIGN SENSITIVITY FORMULATION FOR ELASTOPLASTICITY IN FINITE DEFORMATION

Consider a structure experiencing a finite deformation. Let $\mathbf{X}$ be the material point in the undeformed configuration and $\mathbf{x}$ be the material point in the current configuration with relation of $\mathbf{x} = \mathbf{X} + \mathbf{z}$. The boundary Γ of domain Ω is decomposed of traction boundary Γ_T and the essential boundary Γ_g such that $\Gamma = \Gamma_T \cup \Gamma_g$ and $\Gamma_T \cap \Gamma_g = \emptyset$. The weak formulation of the structural problem is: for given $\mathbf{f}^B, \mathbf{f}^S$, and $\mathbf{z}$, find the displacement function $\mathbf{z}(\mathbf{x}; \mathbf{u}) \in V$ such that

$$a_{\mathbf{u}}(\mathbf{z}, \bar{\mathbf{z}}) = \ell_{\mathbf{u}}(\bar{\mathbf{z}}), \quad \forall \bar{\mathbf{z}} \in Z \tag{1}$$

where $Z = \{\bar{\mathbf{z}}(\mathbf{x}) \in H^1(\Omega) \mid \bar{\mathbf{z}}(\mathbf{x}) = \mathbf{0}, \mathbf{x} \in \Gamma_g\}$ is the space of the kinematically admissible displacement, $V = \{\mathbf{z}(\mathbf{x}; \mathbf{u}) \in H^1(\Omega) \mid \mathbf{z}(\mathbf{x}; \mathbf{u}) = \boldsymbol{\zeta}(\mathbf{x}; \mathbf{u}), \mathbf{x} \in \Gamma_g\}$ is the solution space, $\mathbf{f}^B$ is the body force, $\mathbf{f}^S$ is the surface traction force, $\boldsymbol{\zeta}$ is the prescribed displacement vector, $\bar{\mathbf{z}}$ is the displacement variation, and $\mathbf{u}$ denotes the design vector that is fixed in response analysis. Here $H^1(\Omega)$ denotes the Sobolev space of order one. The subscript $\mathbf{u}$ denotes dependence of the variational form on the design vector $\mathbf{u}$. The variational equation (1) satisfies for any configuration during process. In this paper, the updated Lagrangian formulation is used. In Equation (1),

$$a_{\mathbf{u}}(\mathbf{z}, \bar{\mathbf{z}}) \equiv \int_{\Omega_X} \boldsymbol{\tau} : \bar{\boldsymbol{\varepsilon}} \, d\Omega \tag{2}$$

$$\ell_{\mathbf{u}}(\bar{\mathbf{z}}) = \int_{\Omega_X} \bar{\mathbf{z}}^T \mathbf{f}^B \, d\Omega + \int_{\Gamma_T} \bar{\mathbf{z}}^T \mathbf{f}^S \, d\Gamma \tag{3}$$

are the structural energy form and external load form, and Ω_X is the undeformed domain. $a_{\mathbf{u}}(\mathbf{z}, \bar{\mathbf{z}})$ represents an elastoplastic constitutive relation with Kirchhoff stress $\boldsymbol{\tau} = \boldsymbol{\sigma} \det(\mathbf{F})$ in

which $\boldsymbol{\sigma}$ is the Cauchy stress, and the variation of engineering strain $\bar{\boldsymbol{\varepsilon}} = \mathrm{sym}(\nabla_n \bar{\mathbf{z}})$ where $\mathrm{sym}(\cdot)$ denotes a symmetric part of the tensor and $\nabla_n = \partial/\partial \mathbf{x}$ is a spatial gradient operator at the current time t_n. Accordingly, $\nabla_0 = \partial/\partial \mathbf{X}$ represents a material gradient operator at the undeformed configuration. It is assumed for the moment that the external load is deformation independent, i.e., energy conservative. The formulation for the deformation-dependent load is given in Section 4.

For the structural energy form, a hyperelasticity-based elastoplastic constitutive relation with multiplicative decomposition of the deformation gradient $\mathbf{F} = \mathbf{F}^{\mathrm{e}}\mathbf{F}^{\mathrm{p}}$ proposed by Simo [9] is used where $\mathbf{F}^{\mathrm{e}}$ and $\mathbf{F}^{\mathrm{p}}$ are elastic and plastic deformation gradients, respectively. From the isotropic material assumption, the Kirchhoff stress and left Cauchy–Green deformation tensor have the same principal direction:

$$\boldsymbol{\tau} = \sum_{i=1}^{3} \tau_i^{\mathrm{p}} \mathbf{m}^i \tag{4}$$

$$\mathbf{b}^{\mathrm{e}} = \mathbf{F}^{\mathrm{e}}\mathbf{F}^{\mathrm{e}^{\mathrm{T}}} = \sum_{i=1}^{3} v_i^2 \mathbf{m}^i \tag{5}$$

$$\mathbf{e} = \begin{bmatrix} e_1 \\ e_2 \\ e_3 \end{bmatrix} = \begin{bmatrix} \log(v_1) \\ \log(v_2) \\ \log(v_3) \end{bmatrix} \tag{6}$$

where τ_i^{p} is the principal Kirchhoff stress, v_i is the square root of the principal value of $\mathbf{b}^{\mathrm{e}}$, $\mathbf{m}^i = \mathbf{n}^i \otimes \mathbf{n}^i$, and $\mathbf{n}^i$ is the principal direction of $\mathbf{b}^{\mathrm{e}}$ and $\boldsymbol{\tau}$. For a given displacement increment, the Kirchhoff stress is computed by the return mapping algorithm in the principal stress space with the current configuration. This algorithm is the same as infinitesimal elastoplasticity [27] by using the principal stress and logarithmic strain.

The exact tangent stiffness tensor of Equation (2) was obtained in the literature [9] in the updated Lagrangian formulation as

$$\mathbf{c} = \sum_{i=1}^{3}\sum_{j=1}^{3} c_{ij}^{\mathrm{alg}} \mathbf{m}^i \otimes \mathbf{m}^j + 2\sum_{i=1}^{3} \tau_i^{\mathrm{p}} \mathbf{c}_{\mathrm{trial}}^i \tag{7}$$

where $\otimes$ is the tensor product notation, c_{ij}^{alg} is the consistent tangent stiffness tensor in the principal stress space, and $\mathbf{c}_{\mathrm{trial}}^i$ is the same form from the finite elasticity [9]. Only c_{ij}^{alg} depends on the elastoplastic evolution.

The non-linear variational equation (1) is solved using the Newton–Raphson method. The consistent linearization [9] of the non-linear structural energy form becomes

$$a_{\mathbf{u}}^*(\mathbf{z}; \Delta\mathbf{z}, \bar{\mathbf{z}}) = \int_{\Omega_X} [\bar{\boldsymbol{\varepsilon}} : \mathbf{c} : \boldsymbol{\varepsilon}(\Delta\mathbf{z}) + \boldsymbol{\tau} : \boldsymbol{\eta}(\Delta\mathbf{z}, \bar{\mathbf{z}})]\, \mathrm{d}\Omega \tag{8}$$

where $\boldsymbol{\varepsilon}(\Delta\mathbf{z}) = \mathrm{sym}(\nabla_n \Delta\mathbf{z})$ is the engineering strain tensor and $\boldsymbol{\eta}(\Delta\mathbf{z}, \bar{\mathbf{z}}) = \mathrm{sym}(\nabla_n \bar{\mathbf{z}}^{\mathrm{T}} \nabla_n \Delta\mathbf{z})$ is the non-linear strain tensor. The solution procedure is to compute the incremental displacement such that the unbalanced residual of Equation (1) is vanished. Let the current time be denoted

by left superscript n and the current iteration counter be right superscript $k+1$, then the following linear incremental system of equation is solved:

$$a_{\mathbf{u}}^{*}\left({}^{n}\mathbf{z}^{k};\Delta\mathbf{z}^{k+1},\bar{\mathbf{z}}\right)=\ell_{\mathbf{u}}(\bar{\mathbf{z}})-a_{\mathbf{u}}\left({}^{n}\mathbf{z}^{k},\bar{\mathbf{z}}\right),\quad\forall\bar{\mathbf{z}}\in Z \tag{9}$$

and ${}^{n}\mathbf{z}^{k+1}={}^{n}\mathbf{z}^{k}+\Delta\mathbf{z}^{k+1}$. Equation (9) is solved iteratively until the residual force on the right side is vanished. After convergence, the internal plastic evolution variables and the stress-free intermediate configuration are updated. The same analysis procedures are performed until the final configuration is reached. For a detailed procedure of analysis, refer to References [9–13].

The DSA for the die shape parameter is different from the conventional shape DSA where the shape of the structural domain is the design. The integration domain is fixed from a design standpoint and the effect of the design change comes from the contact variational form described in the next section. Thus, the die shape DSA is a sizing design problem in a strict sense. Since no mathematical proof is available for the regularity of the solution of the non-linear variational equation, it is assumed that the solution of the variational equation (1) is differentiable with respect to design, and

$$\mathbf{z}'=\mathbf{z}'(\mathbf{x};\mathbf{u},\delta\mathbf{u})\equiv\left.\frac{\mathrm{d}}{\mathrm{d}\theta}\mathbf{z}(\mathbf{x};\mathbf{u}+\theta\delta\mathbf{u})\right|_{\theta=0} \tag{10}$$

is the first variation of the solution of Equation (1) at design $\mathbf{u}$ and along the direction $\delta\mathbf{u}$ of the design change. Note that $\mathbf{z}'$ is a function of the independent variable $\mathbf{x}$ and the design variable $\mathbf{u}$ at which the variation is evaluated along the direction $\delta\mathbf{u}$ of the design change. An important property of the design variation is that it commutes with the material gradient operator and domain integration as [1]

$$\begin{aligned}(\nabla_0\mathbf{z})' &= \nabla_0\mathbf{z}'\\ \left(\int_{\Omega_X} g\,\mathrm{d}\Omega\right)' &= \int_{\Omega_X} g'\,\mathrm{d}\Omega\end{aligned} \tag{11}$$

It is also assumed that the structural energy form in Equation (2) is differentiable with respect to the design as

$$a'_{\delta\mathbf{u}}(\mathbf{z},\bar{\mathbf{z}})\equiv\left.\frac{\mathrm{d}}{\mathrm{d}\theta}a_{\mathbf{u}+\theta\delta\mathbf{u}}(\tilde{\mathbf{z}},\bar{\mathbf{z}})\right|_{\theta=0} \tag{12}$$

where $\tilde{\mathbf{z}}$ denotes the state $\mathbf{z}$ with dependence on θ suppressed and $\bar{\mathbf{z}}$ is independent of θ. Equation (12) is the first variation with respect to explicit dependence of $a_{\mathbf{u}}(\mathbf{z},\bar{\mathbf{z}})$ on the design $\mathbf{u}$, which is continuous and linear in $\delta\mathbf{u}$. As proven in Haug *et al.* [1], the load linear form is also differentiable with respect to the design. More specifically,

$$\ell'_{\delta\mathbf{u}}(\bar{\mathbf{z}})\equiv\left.\frac{\mathrm{d}}{\mathrm{d}\theta}\ell_{\mathbf{u}+\theta\delta\mathbf{u}}(\bar{\mathbf{z}})\right|_{\theta=0} \tag{13}$$

For the case of the die shape design, Equation (13) vanishes for the conservative load and $a'_{\delta\mathbf{u}}(\mathbf{z},\bar{\mathbf{z}})$ contains the path dependent terms only.

Using the chain rule of differentiation and the definitions of Equations (10) and (12), the first variation of the structural energy form is

$$\frac{\mathrm{d}}{\mathrm{d}\theta} a_{\mathbf{u}+\theta\delta\mathbf{u}}(\mathbf{z}(\mathbf{x};\mathbf{u}+\theta\delta\mathbf{u}),\bar{\mathbf{z}})\bigg|_{\theta=0} = a^{*}_{\mathbf{u}}(\mathbf{z};\mathbf{z}',\bar{\mathbf{z}}) + a'_{\delta\mathbf{u}}(\mathbf{z},\bar{\mathbf{z}}) \tag{14}$$

where $a^{*}_{\mathbf{u}}(\mathbf{z};\mathbf{z}',\bar{\mathbf{z}})$ is the same form as Equation (8) by substituting $\mathbf{z}'$ into $\Delta\mathbf{z}$, and contains implicitly dependent terms on design. Since obtaining $a'_{\delta\mathbf{u}}(\mathbf{z},\bar{\mathbf{z}})$ requires a quite amount of mathematical derivations, a brief procedure is explained in the following.

The hyperelasticity-based constitutive relation is established from the relation of $\boldsymbol{\tau} : \bar{\boldsymbol{\varepsilon}} = \mathbf{S}^{\mathrm{e}} : \bar{\mathbf{E}}^{\mathrm{e}}$ in which $\mathbf{S}^{\mathrm{e}}$ and $\bar{\mathbf{E}}^{\mathrm{e}}$ are the second Piola–Kirchhoff stress and Lagrangian strain in the intermediate configuration. Thus, for DSA purpose, the structural energy form in Equation (2) is transformed into the intermediate configuration (pull-back), and then differentiated with respect to design. To recover the updated Lagrangian formulation, the differentiated structural energy form is re-transformed in the current configuration (push-forward). The design derivative of the elastic trial Lagrangian strain tensor $\mathbf{E}^{\mathrm{e}} = \frac{1}{2}[\mathbf{F}^{\mathrm{e}^{\mathrm{T}}}\mathbf{F}^{\mathrm{e}} - \mathbf{I}]$ in the intermediate configuration is

$$\mathbf{E}^{\mathrm{e}'} = \mathrm{sym}\left(\mathbf{F}^{\mathrm{e}^{\mathrm{T}}}\mathbf{F}^{\mathrm{e}'}\right) \tag{15}$$

and the transformation of Equation (15) into the current configuration leads to

$$\mathbf{F}^{\mathrm{e}^{-\mathrm{T}}}\mathbf{E}^{\mathrm{e}'}\mathbf{F}^{\mathrm{e}^{-1}} = \mathrm{sym}\left(\mathbf{F}^{\mathrm{e}'}\mathbf{F}^{\mathrm{e}^{-1}}\right) \tag{16}$$

Note that the push-forward transformation is from the intermediate configuration to the current configuration. By using $\mathbf{F}^{\mathrm{e}'} = \mathbf{F}'\mathbf{F}^{\mathrm{p}^{-1}} - \mathbf{F}^{\mathrm{e}}\mathbf{F}^{\mathrm{p}'}\mathbf{F}^{\mathrm{p}^{-1}}$ and by defining a path dependent tensor $\mathbf{G} = \mathbf{F}^{\mathrm{e}}\mathbf{F}^{\mathrm{p}'}\mathbf{F}^{-1}$, Equation (16) can be rearranged as

$$\begin{aligned}\mathbf{F}^{\mathrm{e}^{-\mathrm{T}}}\mathbf{E}^{\mathrm{e}'}\mathbf{F}^{\mathrm{e}^{-1}} &= \mathrm{sym}(\mathbf{F}'\mathbf{F}^{-1}) - \mathrm{sym}(\mathbf{G}) \\ &\equiv \boldsymbol{\varepsilon}(\mathbf{z}') + \boldsymbol{\varepsilon}_{\mathrm{p}}(\mathbf{z})\end{aligned} \tag{17}$$

where $\boldsymbol{\varepsilon}(\mathbf{z}') = \mathrm{sym}(\mathbf{F}'\mathbf{F}^{-1})$ is the implicitly dependent term on design and $\boldsymbol{\varepsilon}_{\mathrm{p}}(\mathbf{z}) = -\mathrm{sym}(\mathbf{G})$ is the contribution from the elastic trial intermediate configuration where the path dependency comes from. The trial elastic deformation gradient $\mathbf{F}^{\mathrm{e}}$ must be extracted from response analysis and the derivative of $\mathbf{F}^{\mathrm{p}}$ must be stored from the previous sensitivity procedure. An interesting observation can be made from the comparison of the rate form and multiplicative plasticity: (1) in additive rate-form plasticity, the path dependency is resulting from the design derivative of the stress tensor at the previous time step and, (2) in multiplicative plasticity, the path dependency is due to the transformation between the intermediate and current configurations.

The same procedure must be applied to the variation of the Lagrangian strain tensor $\bar{\mathbf{E}}^{\mathrm{e}} = \frac{1}{2}[\bar{\mathbf{F}}^{\mathrm{e}^{\mathrm{T}}}\mathbf{F}^{\mathrm{e}} + \mathbf{F}^{\mathrm{e}^{\mathrm{T}}}\bar{\mathbf{F}}^{\mathrm{e}}]$ in the intermediate configuration as

$$\mathbf{F}^{\mathrm{e}^{-\mathrm{T}}}\bar{\mathbf{E}}^{\mathrm{e}'}\mathbf{F}^{\mathrm{e}^{-1}} \equiv \boldsymbol{\eta}(\dot{\mathbf{z}},\bar{\mathbf{z}}) + \boldsymbol{\eta}_{\mathrm{P}}(\mathbf{z},\bar{\mathbf{z}}) \tag{18}$$

where $\boldsymbol{\eta}_{\mathrm{P}}(\mathbf{z},\bar{\mathbf{z}}) = -\mathrm{sym}(\nabla_n\bar{\mathbf{z}}\,\mathbf{G} + \nabla_n\bar{\mathbf{z}}^{\mathrm{T}}\mathbf{G})$ is obtained using a similar procedure as $\boldsymbol{\varepsilon}_{\mathrm{P}}(\mathbf{z})$.

With Equations (17) and (18) in hand, the design derivative of the Kirchhoff stress in Equation (4) becomes

$$\boldsymbol{\tau}' = \sum_{i=1}^{3} \left(\tau_i^{\mathrm{p}'} \mathbf{m}^i + \tau_i^{\mathrm{p}} \mathbf{m}^{i'} \right) \tag{19}$$

The design derivative of the principal stress is a function of the principal logarithmic strain. The following relation can be obtained by the chain rule of differentiation and the push-forward operation:

$$\tau_i^{\mathrm{p}'} = \sum_{j=1}^{3} c_{ij}^{\mathrm{alg}} \mathbf{m}^j : [\boldsymbol{\varepsilon}(\mathbf{z}') + \boldsymbol{\varepsilon}_{\mathrm{P}}(\mathbf{z})] + \frac{\partial \tau_i^{\mathrm{p}}}{\partial e^{\mathrm{p}}} e_n^{\mathrm{p}'} + \frac{\partial \tau_i^{\mathrm{p}}}{\partial \boldsymbol{\alpha}} \boldsymbol{\alpha}_n' \tag{20}$$

Since $\mathbf{m}^i$ is only related to the elastic trial state, it is independent of the plastic evolution and its material derivative can be obtained from the derivative of the elastic trial strain, as

$$\mathbf{m}^{i'} = 2\mathbf{c}_{\mathrm{trial}}^i : [\boldsymbol{\varepsilon}(\mathbf{z}') + \boldsymbol{\varepsilon}_{\mathrm{P}}(\mathbf{z})] \tag{21}$$

Thus, the design derivative of the Kirchhoff stress tensor can be expressed in terms of $\mathbf{z}'$, configuration of response analysis, and sensitivity results of the previous time step, as

$$\begin{aligned} \boldsymbol{\tau}' &= \sum_{i=1}^{3} \left[\tau_i^{\mathrm{p}'} \mathbf{m}^i + \tau_i^{\mathrm{p}} \mathbf{m}^{i'} \right] \\ &= \sum_{i=1}^{3} \sum_{j=1}^{3} \left(c_{ij}^{\mathrm{alg}} \mathbf{m}^i \otimes \mathbf{m}^j + 2\tau_i^{\mathrm{p}} \mathbf{c}_{\mathrm{trial}}^i \right) : (\boldsymbol{\varepsilon}(\mathbf{z}') + \boldsymbol{\varepsilon}_{\mathrm{P}}(\mathbf{z})) + \boldsymbol{\tau}^{\mathbf{fic}} \\ &= \mathbf{c} : (\varepsilon(\mathbf{z}') + \varepsilon_{\mathrm{P}}(\mathbf{z})) + \boldsymbol{\tau}^{\mathbf{fic}} \end{aligned} \tag{22}$$

In Equation (22), the effect of internal plastic variables including back-stress $\boldsymbol{\alpha}$ and effective plastic strain e^{p} is denoted by

$$\boldsymbol{\tau}^{\mathbf{fic}} = \sum_{i=1}^{3} \left[\frac{\partial \tau_i^{\mathrm{p}}}{\partial \boldsymbol{\alpha}} \boldsymbol{\alpha}_n' + \frac{\partial \tau_i^{\mathrm{p}}}{\partial e^{\mathrm{p}}} e_n^{\mathrm{p}'} \right] \mathbf{m}^i \tag{23}$$

By combining Equations (18) and (22), the path dependent term on design, called the structural fictitious load form in Equation (14), is obtained as

$$a_{\delta\mathbf{u}}'(\mathbf{z}, \bar{\mathbf{z}}) = \int_{\Omega_X} (\bar{\boldsymbol{\varepsilon}} : \mathbf{c} : \boldsymbol{\varepsilon}_{\mathrm{P}}(\mathbf{z}) + \boldsymbol{\tau} : \boldsymbol{\eta}_{\mathrm{P}}(\mathbf{z}, \bar{\mathbf{z}}) + \bar{\boldsymbol{\varepsilon}} : \boldsymbol{\tau}^{\mathbf{fic}}) \, \mathrm{d}\Omega \tag{24}$$

For any fixed virtual displacement $\bar{\mathbf{z}} \in Z$, the first variation of Equation (1) is taken to obtain the design sensitivity equation

$$a_{\mathbf{u}}^*(\mathbf{z}; \mathbf{z}', \bar{\mathbf{z}}) = \ell_{\delta\mathbf{u}}'(\bar{\mathbf{z}}) - a_{\delta\mathbf{u}}'(\mathbf{z}, \bar{\mathbf{z}}), \quad \forall \bar{\mathbf{z}} \in Z \tag{25}$$

Presuming that the state $\mathbf{z}$ is known as the solution of Equation (1), using the updated Lagrangian formulation, Equation (25) is the variational equation for the design sensitivity $\mathbf{z}'$. Thus, if a direction $\delta\mathbf{u}$ of design change has been selected, Equation (25) is solved to obtain $\mathbf{z}'$. Since $a_{\delta\mathbf{u}}'(\mathbf{z}, \bar{\mathbf{z}})$ depends on the sensitivity results at the previous time step, Equation (25) is

solved at each converged configuration of the response analysis. Note that the linear sensitivity equation (25) uses the same tangent stiffness matrix as response analysis at the converged configuration.

After solving $\mathbf{z}'$, the first variations of the path dependent variables are updated for the sensitivity computation at the next time step. The first variations of the internal plastic variables are

$$\boldsymbol{\alpha}'_{n+1} = \boldsymbol{\alpha}'_n + \left(H_\alpha + \sqrt{\tfrac{2}{3}}\partial H_\alpha \gamma\right)\gamma' \mathbf{N} + H_\alpha \gamma \mathbf{N}' \tag{26}$$

$$e^{\mathrm{p}'}_{n+1} = e^{\mathrm{p}'}_n + \sqrt{\tfrac{2}{3}}\gamma' \tag{27}$$

where H_α and ∂H_α are the plastic hardening modulus and its derivative with respect to e^{p}_n. The plastic consistency parameter γ is obtained from the return-mapping algorithm and $\mathbf{N}$ is the outward unit normal vector of the elastic domain in the principal Kirchhoff stress space. The design variation of γ and $\mathbf{N}$ can be obtained by taking derivative of the return mapping procedure. This procedure is the same as the classical elastoplasticity and these design variations are presented in Reference [27]. In addition to the plastic variables, the variation of the intermediate configuration is updated by using

$$(\mathbf{F}^{\mathrm{p}}_{n+1})' = (\mathbf{F}^{\mathrm{e}^{-1}}_{n+1})'\mathbf{F}_{n+1} + \mathbf{F}^{\mathrm{e}^{-1}}_{n+1}\mathbf{F}'_{n+1} \tag{28}$$

where $\mathbf{F}'_{n+1} = \nabla_{n+1}\mathbf{z}'$ and $(\mathbf{F}^{\mathrm{e}^{-1}}_{n+1})' = -\mathbf{F}^{\mathrm{e}^{-1}}_{n+1}\mathbf{F}^{\mathrm{e}'}_{n+1}\mathbf{F}^{\mathrm{e}^{-1}}_{n+1}$. From the relation $\mathbf{F}^{\mathrm{e}}_{n+1} = \mathbf{f}^{\mathrm{p}}\mathbf{F}_{n+1}\mathbf{F}^{\mathrm{p}^{-1}}_n$, the following relation can be obtained:

$$\mathbf{F}^{\mathrm{e}'}_{n+1} = \mathbf{f}^{\mathrm{p}'}\mathbf{F}_{n+1}\mathbf{F}^{\mathrm{p}^{-1}}_n + \mathbf{f}^{\mathrm{p}}\mathbf{F}'_{n+1}\mathbf{F}^{\mathrm{p}^{-1}}_n + \mathbf{f}^{\mathrm{p}}\mathbf{F}_{n+1}(\mathbf{F}^{\mathrm{p}^{-1}}_n)' \tag{29}$$

where $\mathbf{F}'_{n+1}$ is available by solving design sensitivity equation (25) and $(\mathbf{F}^{\mathrm{p}^{-1}}_n)'$ is stored from DSA of the previous time step. The design derivative of the incremental plastic deformation gradient $\mathbf{f}^{\mathrm{p}}$ can be obtained from the relation of

$$\begin{aligned} \mathbf{f}^{\mathrm{p}} &= \sum_{i=1}^{3} \exp(-\gamma N_i)\mathbf{m}^i \\ \mathbf{f}^{\mathrm{p}'} &= \sum_{i=1}^{3} \exp(-\gamma N_i)\left[\mathbf{m}^{i'} - (\gamma' N_i + \gamma N'_i)\mathbf{m}^i\right] \end{aligned} \tag{30}$$

where γ' and $\mathbf{N}'$ are obtained in the same procedure as the classical elastoplasticity, presented in Reference [27].

3. DIE DESIGN SENSITIVITY FORMULATION FOR A FRICTIONAL CONTACT PROBLEM

Shape design sensitivity formulation for a continuum-based frictional contact problem is presented in References [17, 18]. A die shape design sensitivity formulation is developed in this paper. Figure 1 shows a general contact condition with a rigid wall in R^2. A co-ordinate ξ represents the natural co-ordinate of the rigid surface. The co-ordinate of the contact point $\mathbf{x}_{\mathrm{c}}$

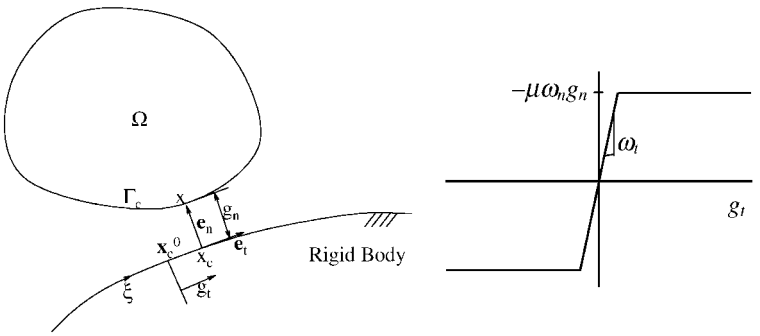

Figure 1. Contact condition using penalty method and friction model.

can be represented using the natural co-ordinate at the contact point ξ_c by $\mathbf{x}_c = \mathbf{x}_c(\xi_c)$. The normal contact condition can be imposed on the structure by measuring the distance between a part of the structural boundary Γ_c at the current configuration and the surface of the rigid wall, whereas the tangential slip condition can be established by measuring the relative slip distance between two consecutive time steps. A contact condition can be defined using the normal gap function g_n and tangential slip function g_t as

$$g_n \equiv (\mathbf{x} - \mathbf{x}_c(\xi_c))^T \mathbf{e}_n(\xi_c) \geqslant 0, \quad \mathbf{x} \in \Gamma_c \tag{31}$$

$$g_t \equiv \|\mathbf{t}^0\|(\xi_c - \xi_c^0) \tag{32}$$

where $\mathbf{e}_n$ and $\mathbf{e}_t$ are the unit outward normal and tangential vectors of the rigid wall at the contact point, respectively, $\|\mathbf{t}^0\|$ is the norm of the tangential vector, and ξ_c^0 is the natural co-ordinate of the previous converged time step. For notational convenience, define several scalar symbols as

$$\begin{aligned} d &\equiv \mathbf{e}_n^T \mathbf{x}_{c,\xi\xi}, \quad \beta \equiv \mathbf{e}_t^T \mathbf{x}_{c,\xi\xi}, \quad \rho \equiv \mathbf{e}_n^T \mathbf{x}_{c,\xi\xi\xi} \\ c &\equiv \|\mathbf{t}\|^2 - g_n \alpha, \quad v \equiv \|\mathbf{t}\|\|\mathbf{t}^0\|/c \end{aligned} \tag{33}$$

The frictional force is bounded above by $-\mu\omega_n g_n$ in the Coulomb friction law. But for the case of small slip (micro-displacement), the traction force is proportional to the tangential slip. The penalty parameter ω_t is a constant for this case. Figure 1 shows a friction curve used in this paper. A stick condition occurs when the frictional traction force is less than the normal force multiplied by the frictional coefficient as $|\omega_t g_t| \leqslant |\mu\omega_n g_n|$. Otherwise, it becomes a slip condition. Thus, the contact variational form can be classified as either a stick or slip condition. By taking the first variation of the standard penalty function, the contact variational form can be obtained as

$$\begin{aligned} b_{\mathbf{u}}(\mathbf{z}, \bar{\mathbf{z}}) &= \omega_n \int_{\Gamma_C} g_n \bar{\mathbf{z}}^T \mathbf{e}_n \, d\Gamma \begin{cases} +\omega_t \displaystyle\int_{\Gamma_C} v g_t \bar{\mathbf{z}}^T \mathbf{e}_t \, d\Gamma & \text{if } |\omega_t g_t| \leqslant |\mu\omega_n g_n| \\ -\mu\omega_n \mathrm{sgn}(g_t) \displaystyle\int_{\Gamma_C} v g_n \bar{\mathbf{z}}^T \mathbf{e}_t \, d\Gamma & \text{otherwise} \end{cases} \\ &\equiv b_N(\mathbf{z}, \bar{\mathbf{z}}) + b_T(\mathbf{z}, \bar{\mathbf{z}}) \end{aligned} \tag{34}$$

where $b_N(\mathbf{z},\bar{\mathbf{z}})$ is the normal contact variational form and $b_T(\mathbf{z},\bar{\mathbf{z}})$ is the tangential stick/slip variational form. The contact variational form in Equation (34) is non-linear with respect to the displacement. The linearization of the contact variational form in Equation (34) leads to the contact bilinear form defined as [17]

$$b^*_{\mathbf{u}}(\mathbf{z};\Delta\mathbf{z},\bar{\mathbf{z}}) = b^*_N(\mathbf{z};\Delta\mathbf{z},\bar{\mathbf{z}}) + b^*_T(\mathbf{z};\Delta\mathbf{z},\bar{\mathbf{z}}) \tag{35}$$

where

$$b^*_N(\mathbf{z};\Delta\mathbf{z},\bar{\mathbf{z}}) = \omega_n \int_{\Gamma_C} \bar{\mathbf{z}}^{\mathrm{T}}\mathbf{e}_n\mathbf{e}_n^{\mathrm{T}}\Delta\mathbf{z}\,d\Gamma - \omega_n \int_{\Gamma_C} (d g_n/c)\bar{\mathbf{z}}^{\mathrm{T}}\mathbf{e}_t\mathbf{e}_t^{\mathrm{T}}\Delta\mathbf{z}\,d\Gamma \tag{36}$$

$$\begin{aligned} b^*_T(\mathbf{z};\Delta\mathbf{z},\bar{\mathbf{z}}) = {} & \omega_t \int_{\Gamma_C} v^2\bar{\mathbf{z}}^{\mathrm{T}}\mathbf{e}_t\mathbf{e}_t^{\mathrm{T}}\Delta\mathbf{z}\,d\Gamma \\ & + \omega_t \int_{\Gamma_C} (d v\, g_t/c)\bar{\mathbf{z}}^{\mathrm{T}}\left(\mathbf{e}_n\mathbf{e}_t^{\mathrm{T}} + \mathbf{e}_t\mathbf{e}_n^{\mathrm{T}}\right)\Delta\mathbf{z}\,d\Gamma \\ & + \omega_t \int_{\Gamma_C} \left(v g_t/c^2\right)\left[(\rho\,\|\mathbf{t}\| - 2\,d\beta)g_n - \beta\|\mathbf{t}\|^2\right]\bar{\mathbf{z}}^{\mathrm{T}}\mathbf{e}_t\mathbf{e}_t^{\mathrm{T}}\Delta\mathbf{z}\,d\Gamma \quad \text{if } |\omega_t g_t| \leqslant |\mu\omega_n g_n| \end{aligned} \tag{37}$$

$$\begin{aligned} b^*_T(\mathbf{z};\Delta\mathbf{z},\bar{\mathbf{z}}) = {} & \omega_t \int_{\Gamma_C} v\bar{\mathbf{z}}^{\mathrm{T}}\mathbf{e}_t\mathbf{e}_n^{\mathrm{T}}\Delta\mathbf{z}\,d\Gamma \\ & + \omega_t \int_{\Gamma_C} (d v\, g_n/c)\bar{\mathbf{z}}^{\mathrm{T}}\left(\mathbf{e}_n\mathbf{e}_t^{\mathrm{T}} + \mathbf{e}_t\mathbf{e}_n^{\mathrm{T}}\right)\Delta\mathbf{z}\,d\Gamma \\ & + \omega_t \int_{\Gamma_C} \left(v g_n/c^2\right)\left[(\rho\|\mathbf{t}\| - 2d\beta)g_n - \beta\|\mathbf{t}\|^2\right]\bar{\mathbf{z}}^{\mathrm{T}}\mathbf{e}_t\mathbf{e}_t^{\mathrm{T}}\Delta\mathbf{z}\,d\Gamma \quad \text{if } |\omega_t g_t| > |\mu\omega_n g_n| \end{aligned} \tag{38}$$

where for the case of the slip contact condition, the tangential penalty parameter ω_t is related to the normal penalty parameter ω_n by $\omega_t = -\mu\omega_n\,\mathrm{sgn}(g_t)$. For the case of the stick condition, the contact bilinear form equation (35) is symmetric with respect to the incremental displacement and the variation of the displacement. This is expected since the contact phenomena for a stick condition are energy conservative. For the case of the slip condition, the contact bilinear form equation (35) is not symmetric. The system is no longer conservative if it starts to slip along the master surface. To obtain the total linearized system of equations including contact, Equation (35) is combined with structural equation (9) as

$$a^*_{\mathbf{u}}\left({}^n\mathbf{z}^k;\Delta\mathbf{z}^{k+1},\bar{\mathbf{z}}\right) + b^*_{\mathbf{u}}\left({}^n\mathbf{z}^k;\Delta\mathbf{z}^{k+1},\bar{\mathbf{z}}\right) = \ell_{\mathbf{u}}(\bar{\mathbf{z}}) - a_{\mathbf{u}}\left({}^n\mathbf{z}^k,\bar{\mathbf{z}}\right) - b_{\mathbf{u}}\left({}^n\mathbf{z}^k,\bar{\mathbf{z}}\right), \quad \forall\bar{\mathbf{z}} \in Z \tag{39}$$

The design sensitivity formulation for a contact problem uses the same linearization method as the structural energy form. The die shape change can be treated easily using the concept of the shape perturbation and design velocity. Let the geometry of the rigid surface be perturbed in the direction of $\mathbf{V}_c(\xi)$ (design velocity) which corresponds to the design change $\delta\mathbf{u}$. The contact variational form in Equation (34) is differentiated with respect to the design perturbation at the original geometry to construct a design sensitivity equation.

The variations of the normal contact and tangential slip variational forms become

$$(b_N(\mathbf{z},\bar{\mathbf{z}}))' \equiv b_N^*(\mathbf{z};\mathbf{z}',\bar{\mathbf{z}}) + b_N'(\mathbf{z},\bar{\mathbf{z}}) \tag{40}$$

$$(b_T(\mathbf{z},\bar{\mathbf{z}}))' = b_T^*(\mathbf{z};\mathbf{z}',\bar{\mathbf{z}}) + b_T'(\mathbf{z},\bar{\mathbf{z}}) \tag{41}$$

where

$$b_N'(\mathbf{z},\bar{\mathbf{z}}) = -b_N^*(\mathbf{z};\mathbf{V}_c,\bar{\mathbf{z}}) - \omega_n \int_{\Gamma_C} (g_n\|\mathbf{t}\|/c)\bar{\mathbf{z}}^T\mathbf{e}_t\mathbf{e}_n^T\mathbf{V}_{c,\xi}\,d\Gamma \tag{42}$$

$$\begin{aligned} b_T'(\mathbf{z},\bar{\mathbf{z}}) = {} & -b_T^*(\mathbf{z};\mathbf{V}_c,\bar{\mathbf{z}}) + \omega_t \int_{\Gamma_C} (2g_t\|\mathbf{t}\|/c)\,\bar{\mathbf{z}}^T\mathbf{e}_t\mathbf{e}_t^{0^T}\mathbf{V}_{c,\xi}\,d\Gamma \\ & + \omega_t \int_{\Gamma_C} v(2\beta^0 g_t - \|\mathbf{t}^0\|^2)\,\bar{\mathbf{z}}^T\mathbf{e}_t\mathbf{e}_t^{0^T}(\dot{\mathbf{z}}^0 - \mathbf{V}_c)\,d\Gamma \\ & + \omega_t \int_{\Gamma_C} (\beta^0 g_n g_t(\|\mathbf{t}^0\| + \|\mathbf{t}\|)/cc^0)\,\bar{\mathbf{z}}^T\mathbf{e}_t\mathbf{e}_n^{0^T}\mathbf{V}_{c,\xi}\,d\Gamma \\ & - \omega_t \int_{\Gamma_C} (g_n\|\mathbf{t}\|\|\mathbf{t}^0\|^2/cc^0)\,\bar{\mathbf{z}}^T\mathbf{e}_t\mathbf{e}_n^{0^T}\mathbf{V}_{c,\xi}\,d\Gamma \quad \text{if } |\omega_t g_t| \leqslant |\mu\omega_n g_n| \end{aligned} \tag{43}$$

$$\begin{aligned} b_T'(\mathbf{z},\bar{\mathbf{z}}) = {} & -b_T^*(\mathbf{z};\mathbf{V}_c,\bar{\mathbf{z}}) \\ & + \omega_t \int_{\Gamma_C} (g_n\|\mathbf{t}\|/c)\,\bar{\mathbf{z}}^T\mathbf{e}_t\mathbf{e}_t^{0^T}\mathbf{V}_{c,\xi}\,d\Gamma \\ & + \omega_t \int_{\Gamma_C} (v\beta^0 g_n/c)\,\bar{\mathbf{z}}^T\mathbf{e}_t\mathbf{e}_t^{0^T}(\dot{\mathbf{z}}^0 - \mathbf{V}_c)\,d\Gamma \\ & + \omega_t \int_{\Gamma_C} (\beta^0 g_n g_n^0\|\mathbf{t}^0\|/cc^0)\,\bar{\mathbf{z}}^T\mathbf{e}_t\mathbf{e}_n^{0^T}\mathbf{V}_{c,\xi}\,d\Gamma \quad \text{if } \omega_t g_t| > |\mu\omega_n g_n| \end{aligned} \tag{44}$$

The design derivatives of the contact variational form can be obtained from Equations (40) through (44) as

$$\frac{d}{d\theta} b_{\mathbf{u}+\theta\delta\mathbf{u}}(\mathbf{z}(\mathbf{x};\mathbf{u}+\theta\delta\mathbf{u}),\bar{\mathbf{z}})\bigg|_{\theta=0} = b_{\mathbf{u}}^*(\mathbf{z};\mathbf{z}',\bar{\mathbf{z}}) + b_{\delta\mathbf{u}}'(\mathbf{z},\bar{\mathbf{z}}) \tag{45}$$

$$b_{\mathbf{u}}^*(\mathbf{z};\mathbf{z}',\bar{\mathbf{z}}) = b_N^*(\mathbf{z};\mathbf{z}',\bar{\mathbf{z}}) + b_T^*(\mathbf{z};\mathbf{z}',\bar{\mathbf{z}}) \tag{46}$$

$$b_{\delta\mathbf{u}}'(\mathbf{z},\bar{\mathbf{z}}) = b_N'(\mathbf{z},\bar{\mathbf{z}}) + b_T'(\mathbf{z},\bar{\mathbf{z}}) \tag{47}$$

where $b_{\mathbf{u}}^*(\mathbf{z};\mathbf{z}',\bar{\mathbf{z}})$ has same expression as Equation (35) by substituting $\Delta\mathbf{z}$ into $\mathbf{z}'$ and $b_{\delta\mathbf{u}}'(\mathbf{z},\bar{\mathbf{z}})$ is contact fictitious load that represents explicit/path dependent terms on design.

By combining the variation of the contact variational form in Equation (45) with that of structure in Equations (25), the following design sensitivity equation is obtained:

$$a_{\mathbf{u}}^*(\mathbf{z};\mathbf{z}',\bar{\mathbf{z}}) + b_{\mathbf{u}}^*(\mathbf{z};\mathbf{z}',\bar{\mathbf{z}}) = \ell_{\delta\mathbf{u}}'(\bar{\mathbf{z}}) - a_{\delta\mathbf{u}}'(\mathbf{z},\bar{\mathbf{z}}) - b_{\delta\mathbf{u}}'(\mathbf{z},\bar{\mathbf{z}}), \quad \forall\bar{\mathbf{z}} \in Z \tag{48}$$

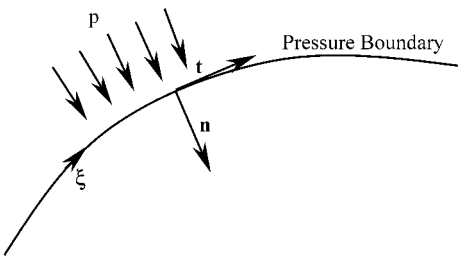

Figure 2. Pressure boundary load condition.

The linearized design sensitivity equation (48) is solved at each converged configuration without iteration. Since the left-hand side is the same as that of Equation (39), the decomposed tangent stiffness matrix of response analysis is used for sensitivity computation very efficiently.

4. DESIGN SENSITIVITY ANALYSIS OF BOUNDARY PRESSURE LOAD

The pressure load is frequently used in the metal forming process. It can be used as an active loading method in the hydro-forming process or used as a supporting pressure to improve quality of product in the deepdrawing process. In this section, a brief derivation of the linearization of the boundary pressure load in R^2 is presented. By introducing a parametric representation, the transformation to the undeformed configuration is avoided. Moreover, a very simple DSA formulation can be obtained because the design derivative commutes with the parameter integration. Let the current pressure boundary be Γ_x and the constant pressure be p. The external load form for this case is

$$\ell_{\mathbf{u}}(\mathbf{z}, \bar{\mathbf{z}}) = \int_{\Gamma_x} p\bar{\mathbf{z}}^{\mathrm{T}}\mathbf{e}_n \, \mathrm{d}\Gamma_x \tag{49}$$

where $\mathbf{e}_n$ is a unit inward normal of the current pressure boundary. The notation $\ell_{\mathbf{u}}(\mathbf{z}, \bar{\mathbf{z}})$ is used instead of the usual notation $\ell_{\mathbf{u}}(\bar{\mathbf{z}})$ since the pressure load direction depends on the displacement $\mathbf{z}$ implicitly. As a usual procedure, this spatial formulation can be transformed to the undeformed configuration using the Nanson's formula,

$$\mathbf{e}_n \, \mathrm{d}\Gamma_x = J\mathbf{F}^{-\mathrm{T}}\mathbf{E}_n \, \mathrm{d}\Gamma_X \tag{50}$$

where $J = |\mathbf{F}|$, $\mathbf{F}$ is the deformation gradient, and $\mathbf{E}_n$ is a unit inward normal at the undeformed configuration. The linearization of this formula requires computation of the curvature on the boundary, which is not a trivial procedure. Instead of using Equation (50), the parametric representation method is proposed below.

As shown in Figure 2, let the pressure boundary be parameterized by ξ. The tangent vector and inward normal vector can be defined by the derivative of the boundary point $\mathbf{x} \in \Gamma_x$ with respect to the parameter ξ as

$$\begin{aligned} \mathbf{t} &= \mathbf{x}_{,\xi} \\ \mathbf{n} &= -\mathbf{e}_3 \times \mathbf{t} = \mathbf{R}\mathbf{x}_{,\xi} \end{aligned} \tag{51}$$

where $\mathbf{R}$ is an orthogonal rotation matrix. It can be shown that $\mathbf{e}_n \, \mathrm{d}\Gamma_x = \mathbf{n} \, \mathrm{d}\xi$. Thus, the external load form in Equation (49) can be expressed using Equation (51) in the parametric space by

$$\ell_{\mathbf{u}}(\mathbf{z}, \bar{\mathbf{z}}) = \int_{\xi} p \bar{\mathbf{z}}^{\mathrm{T}} \mathbf{R} \, \mathbf{x}_{,\xi} \, \mathrm{d}\xi \tag{52}$$

The linearization of $\ell_{\mathbf{u}}(\mathbf{z}, \bar{\mathbf{z}})$ depends only on $\mathbf{x}_{,\xi}$, and by using $\Delta(\mathbf{x}_{,\xi}) = \Delta \mathbf{z}_{,\xi}$,

$$\ell^*_{\mathbf{u}}(\Delta \mathbf{z}, \bar{\mathbf{z}}) = \int_{\xi} p \bar{\mathbf{z}}^{\mathrm{T}} \mathbf{R} \, \Delta \mathbf{z}_{,\xi} \, \mathrm{d}\xi \tag{53}$$

which is the linearized boundary pressure load or load correction form. Let the current time be t_n and the current iteration count be $k+1$; the linearized variational equation for the structure with the pressure boundary load can be written as

$$\begin{aligned} &a^*_{\mathbf{u}}({}^n\mathbf{z}^k; \Delta \mathbf{z}^{k+1}, \bar{\mathbf{z}}) + b^*_{\mathbf{u}}({}^n\mathbf{z}^k; \Delta \mathbf{z}^{k+1}, \bar{\mathbf{z}}) - \ell^*_{\mathbf{u}}(\Delta \mathbf{z}^{k+1}, \bar{\mathbf{z}}) \\ &\quad = \ell_{\mathbf{u}}({}^n\mathbf{z}^k, \bar{\mathbf{z}}) - a_{\mathbf{u}}({}^n\mathbf{z}^k, \bar{\mathbf{z}}) - b_{\mathbf{u}}({}^n\mathbf{z}^k, \bar{\mathbf{z}}), \quad \forall \bar{\mathbf{z}} \in Z \end{aligned} \tag{54}$$

A good feature of the parametric representation is that the parameter is independent of the deformation and design perturbation. The design variation can be brought inside the parameter integration. The design variation of the load linear form in Equation (52) becomes

$$\frac{\mathrm{d}}{\mathrm{d}\theta} \ell_{\mathbf{u}+\theta\delta\mathbf{u}}(\mathbf{z}(\mathbf{x}; \mathbf{u} + \theta\delta\mathbf{u}), \bar{\mathbf{z}}) \bigg|_{\theta=0} = \ell^*_{\mathbf{u}}(\mathbf{z}', \bar{\mathbf{z}}) + \ell'_{\delta\mathbf{u}}(\mathbf{z}, \bar{\mathbf{z}}) \tag{55}$$

where

$$\ell'_{\delta\mathbf{u}}(\mathbf{z}, \bar{\mathbf{z}}) = \int_{\xi} \bar{\mathbf{z}}^{\mathrm{T}} \mathbf{n} \, \delta p \, \mathrm{d}\xi \tag{56}$$

is the fictitious load form due to the pressure load when the pressure is a design parameter. The effect of $\ell'_{\delta\mathbf{u}}(\mathbf{z}, \bar{\mathbf{z}})$ vanishes for the die shape design. However, $\ell^*_{\mathbf{u}}(\mathbf{z}', \bar{\mathbf{z}})$ is required to compute the sensitivity equation. The design sensitivity equation is obtained from Equations (48) and (55) as

$$a^*_{\mathbf{u}}(\mathbf{z}; \mathbf{z}', \bar{\mathbf{z}}) + b^*_{\mathbf{u}}(\mathbf{z}; \mathbf{z}', \bar{\mathbf{z}}) - \ell^*_{\mathbf{u}}(\mathbf{z}', \bar{\mathbf{z}}) = \ell'_{\delta\mathbf{u}}(\mathbf{z}, \bar{\mathbf{z}}) - a'_{\delta\mathbf{u}}(\mathbf{z}, \bar{\mathbf{z}}) - b'_{\delta\mathbf{u}}(\mathbf{z}, \bar{\mathbf{z}}), \quad \forall \bar{\mathbf{z}} \in Z \tag{57}$$

5. NUMERICAL EXAMPLE: DIE SHAPE OPTIMIZATION OF SHEET METAL STAMPING PROCESS

The meshfree methods were developed recently to remove or reduce the mesh dependence of the conventional finite element method. In the meshfree method, the shape function is not a function of the referential co-ordinate but a function of the spatial co-ordinate, and the order of completeness in the approximation can be customized easily. Insensitivity to the mesh distortion is a very important feature in non-linear analysis and shape design optimization, in addition to the high accuracy in the meshfree method. Higher accuracy can be achieved by

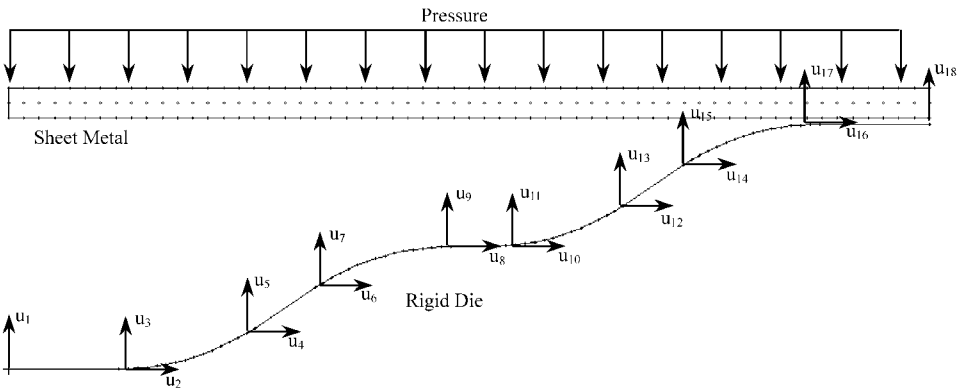

Figure 3. Design parameterization of sheet metal stamping problem.

simply adding more nodes to the structure without re-modelling the total structure. However, the difficulty in imposing the essential boundary condition and relatively high cost of analysis are weaknesses in spite of the aforementioned advantages. The domain partitioning for domain integration is independent of the nodal locations, and nodes are not interconnected by elements. The response variables like displacements are defined at the nodes and are independent of the integration zones. In this paper the reproducing kernel particle method (RKPM) developed by Liu *et al.* [24] is used as the analysis tool. For detailed explanations of the domain partitioning and construction of meshfree shape function, refer to References [24–26]. A concept of Lagrangian kernel [25, 26] is important in obtaining stable solutions in large deformation problems. Imposition of the boundary condition has been improved by a mixed transformation method and a boundary singular kernel method [27, 28]. For other applications of the meshfree method DSA, refer to Reference [27].

A pressurized metal stamping process has been proven to be effective in the manufacturing process. The applied pressure is always normal to the workpiece to give an even distribution of the normal stress, whereas a conventional stamping process using two rigid dies applies force only to the direction of die movement. This feature reduces the local concentration of the plastic flow and, thus, prevents the necking phenomena. The example in this paper simulates the manufacturing process of the sheet metal stamping based on a quasi-static assumption and DSA of the final shape of the workpiece with respect to the die shape parameters. The desirable shape of the workpiece after spring-back can be obtained by changing the shape of the rigid die. The geometry of the workpiece is represented by 183 RKPM particles as shown in Figure 3. In the thickness direction, three particles are used. The rigid die is modelled with 65 piecewise linear master segments and the frictional contact condition is established between the slave nodes on the bottom surface of the workpiece and the master segments. A symmetric boundary condition is applied at the left end of the workpiece. A constant pressure of 70 MPa is applied at the top surface of the workpiece and then removed to observe the spring-back amount.

It is assumed that the pressure is applied very slowly such that the quasi-static analysis can be used. The frictional contact conditions are established between the rigid die and the workpiece at the bottom surface using the contact penalty parameter $\omega_n = 10^5$ and the

friction coefficient $\mu = 0.4$. Finite deformation elastoplasticity with multiplicative decomposition of the deformation gradient is used as a constitutive model with Young's modulus $E = 206.9$ GPa, Poisson's ratio $v = 0.29$, plastic hardening modulus $H_\alpha = 1.1$ GPa, and initial yield stress $\sigma_y = 0.5$ GPa. Linear isotropic hardening is used, and therefore the plastic consistency condition can be solved explicitly without iteration.

Non-linear response analysis is carried out using the standard Newton–Raphson method with 300 load steps. After the solution is converged at each load step, the decomposed tangent stiffness matrix is stored for DSA. The intermediate configuration and internal plastic variables are updated following DSA. Plate 1 shows the contour plot of the effective plastic strain at the final converged configuration after pressure is removed. The amount of spring-back is about 0.56 cm at the lower-left corner of the workpiece, and a relatively large spring-back occurred around the concave regions.

The geometry of the rigid die is represented by cubic spline curves, and each point on the boundary has a unique parametric representation. The locations of the control points of each curve are chosen as design parameters. The design velocity vector corresponding to the particle point can be computed using the parametric representation. Eighteen design parameters are chosen as shown in Figure 3. After design parameters are selected, the design velocity field is obtained by perturbing the geometric curve along the direction of each design parameters.

Using the design velocity information, DSA is carried out. Since the constitutive model is based on the finite deformation elastoplasticity with multiplicative decomposition of the deformation gradient, the sensitivity formulation is path dependent and is solved at each converged load step. The frictional contact also contributes to the path dependency of the design sensitivity. After response analysis is converged at each load step, the decomposed tangent stiffness matrix is stored for the sensitivity procedure. Using the response analysis results, design velocity, and design variation of the intermediate configuration and internal state variables, the structural fictitious load form in Equation (24) is computed. In addition, the contribution of the contact fictitious load is computed using Equation (47). The linear system of Equation (57) is solved using the decomposed tangent stiffness matrix from response analysis and the fictitious load. No iteration is required to solve the design sensitivity equation (57), and this equation is solved for the number of design parameters. Thus, the LU decomposition of the tangent stiffness matrix is important. This procedure is quite efficient compared to iterative response analysis. The design sensitivity equation solves for the design variation $\mathbf{z}'$ of the displacement.

After computing $\mathbf{z}'$, design variations of the intermediate configuration and internal plastic variables are updated using $\mathbf{z}'$. The sensitivity coefficients of the performance measures are computed after solving the design sensitivity equation at the final converged load step. Performance measures that can be considered in this approach are the displacement, stress tensor, internal plastic variables, reaction force, contact force, and normal gap distance.

The response analysis is carried out in 2843 s of CPU time, whereas DSA requires 2350 s for 18 design parameters, which is less than 5 per cent of the response analysis time per design parameter. This efficiency is because the sensitivity equation is solved without iteration and it uses the decomposed tangent stiffness matrix from the response analysis. Table I shows the sensitivity coefficients and comparison of the sensitivity results with the finite difference results. The third column $\Delta\Psi$ denotes the first-order sensitivity results from the forward finite difference method with perturbation of $\theta = 10^{-6}$, and the fourth column represents the sensitivity result by the proposed method. Very good agreement is observed between sensitivity solutions and finite difference results. e^{p} in the first column of Table I represents the effective

Table I. Comparison of DSA results with finite difference methods.

Performance	(Ψ)	$\Delta\Psi$	Ψ'	$(\Delta\Psi/\Psi') \times 100\%$
u_1				
e_{28}^{p}	0.118906E+00	−0.194252E−08	−0.194252E−08	100.00
e_{49}^{p}	0.104386E+00	0.798968E−09	0.798972E−09	100.00
e_{55}^{p}	0.754636E−01	0.388700E−08	0.388699E−08	100.00
e_{68}^{p}	0.125680E+00	−0.193967E−08	−0.193967E−08	100.00
e_{70}^{p}	0.130504E+00	−0.253478E−09	−0.253473E−09	100.00
G	0.897186E+01	0.800142E−06	0.759230E−06	105.39
u_3				
e_{28}^{p}	0.118906E+00	−0.119749E−09	−0.119754E−09	100.00
e_{49}^{p}	0.104386E+00	0.163800E−08	0.163800E−08	100.00
e_{55}^{p}	0.754636E−01	−0.297925E−08	−0.297925E−08	100.00
e_{68}^{p}	0.125680E+00	−0.874930E−09	−0.874917E−09	100.00
e_{70}^{p}	0.130504E+00	−0.235636E−09	−0.235632E−09	100.00
G	0.897186E+01	−0.172934E−05	−0.155892E−05	110.93
u_5				
e_{28}^{p}	0.18906E+00	−0.100967E−10	−0.101010E−10	99.96
e_{49}^{p}	0.104386E+00	0.962387E−09	0.962387E−09	100.00
e_{55}^{p}	0.754636E−01	−0.161494E−08	−0.161495E−08	100.00
e_{68}^{p}	0.125680E+00	−0.445413E−09	−0.445412E−09	100.00
e_{70}^{p}	0.130504E+00	−0.174951E−10	−0.174948E−10	100.00
G	0.897186E+01	−0.483547E−06	−0.484111E−06	99.88
u_7				
e_{28}^{p}	0.118906E+00	0.815986E−09	0.815981E−09	100.00
E_{49}^{p}	0.104386E+00	−0.309183E−08	−0.309183E−08	100.00
e_{55}^{p}	0.754636E−01	0.391398E−08	0.391397E−08	100.00
e_{68}^{p}	0.125680E+00	−0.156687E−07	−0.156687E−07	100.00
e_{70}^{p}	0.130504E+00	−0.132360E−07	−0.132360E−07	100.00
G	0.897186E+01	0.124364E−05	0.112289E−05	110.75
u_9				
e_{28}^{p}	0.118906E+00	0.618719E−09	0.618714E−09	100.00
e_{49}^{p}	0.104386E+00	0.369257E−08	0.369257E−08	100.00
e_{55}^{p}	0.754636E−01	−0.122360E−08	−0.122361E−08	100.00
e_{68}^{p}	0.125680E+00	0.249702E−07	0.249702E−07	100.00
e_{70}^{p}	0.130504E+00	0.109689E−07	0.109689E−07	100.00
G	0.897186E+01	0.271127E−05	0.272400E−05	99.53

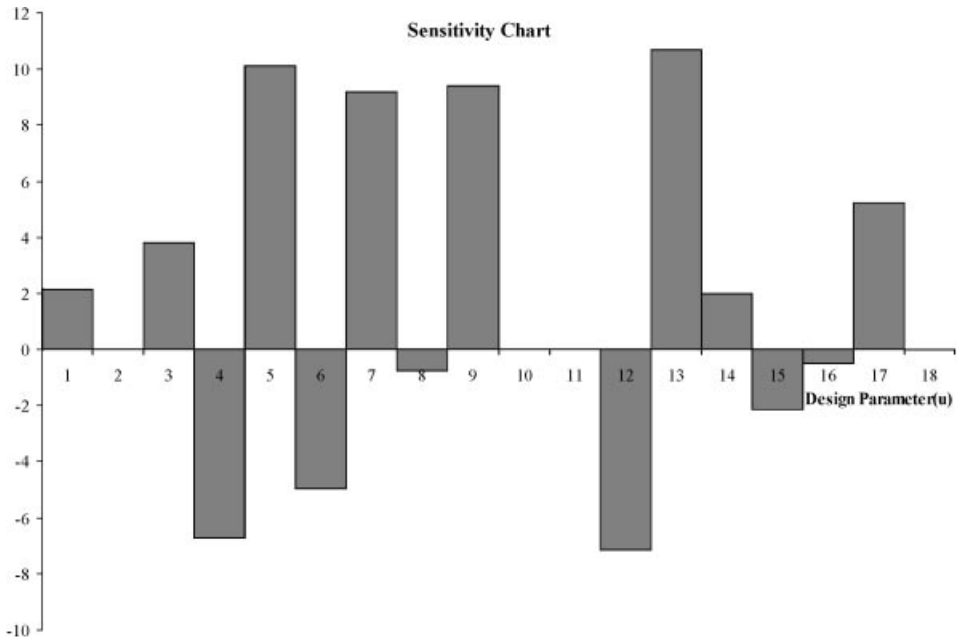

Figure 4. Design sensitivity chart for shape difference with respect to design parameters.

plastic strain at the integration zone and G denotes the square sum of the normal distance between the desirable shape and the final geometry of the workpiece defined by

$$G = \sum_{I}^{\mathrm{NP}} \|\pi(\mathbf{x}_I) - \mathbf{x}_I\|^2 \tag{58}$$

where $\pi(\mathbf{x}_I)$ is the normal projection of $\mathbf{x}_I$ onto the predetermined surface Γ and NP is the number of particles in the bottom surface of the workpiece. This parameter G is used for the minimization of spring-back in the subsequent design optimization. Figure 4 shows a sensitivity chart of G in Equation (58) with respect to 18 design parameters. It is clear how the performance measure is influenced by the change of design parameters.

The final deformed shape of the workpiece in Plate 1 is different from the desired shape because of the elastic spring-back effect. For the die design optimization, the initial shape of the rigid die is selected as the desired final shape of the workpiece. The design objective is to match the shape of the workpiece with the desired geometry after removing the pressure load. The design optimization problem can be formulated such that the normal distance between the final shape of the workpiece and the desired shape is minimized. Since the possibility of the material failure and necking of the workpiece increases as the magnitude of the effective plastic strain increases, the magnitude of the effective plastic strain is maintained through the design constraints. Equation (59) shows the design formulation with eight constraints for the effective plastic strain. The design parameters, which are the locations of the control points

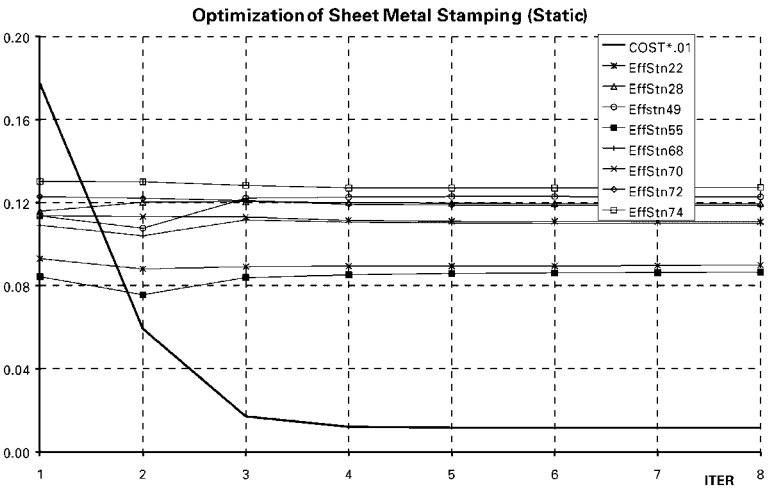

Figure 5. Optimization history of cost and constraints functions.

of the spline curves, are allowed to move between -2 and 2:

$$\begin{aligned} &Min \quad G \\ &s.t. \quad e_i^{\mathrm{p}} \leqslant 0.13, \quad i = 22, 28, 49, 55, 68, 70, 72, 74 \\ &\qquad -2.0 \leqslant u_j \leqslant 2.0, \quad j = 1, \ldots, 18 \end{aligned} \tag{59}$$

Design optimization is carried out using the sequential quadratic programming method in DOT [30]. The performance values are supplied to the DOT from non-linear response analysis (RKPM), and the sensitivity coefficients are provided by the proposed method. The initial design is feasible and all constraints on effective plastic strain are satisfied. An optimization problem converges after eight iterations and all constraints are satisfied. The cost function, which is the square sum of the normal distances between the final shape of the workpiece and the desired shape, is reduced up to 10 per cent of the original design. All the constraints are maintained at the same levels as those in the initial design.

Figure 5 shows the optimization history of the cost and constraint functions. Straightforward convergence is observed even though the response analysis displays many non-linearities. The cost function is reduced greatly at the first four iterations and most of the constraints remain constant. Figure 6 shows the optimized design of the rigid die. The optimization algorithm increases the curvature of the rigid die around the concave region to obtain the desired shape after the elastic spring-back of the workpiece. Plate 2 shows the results of the response analysis at the optimum design. The final shape of the workpiece after spring-back is well matched with the desired shape.

6. CONCLUSION AND FUTURE PLAN

A die shape design sensitivity analysis is proposed for design optimization of the manufacturing process. The sizing design sensitivity equation is obtained by taking the derivative of

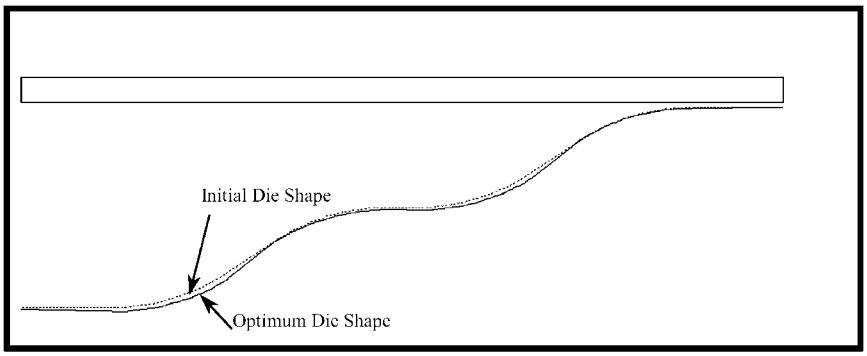

Figure 6. Optimized die shape for sheet metal stamping.

the non-linear continuum variational equation with respect to die shape design parameters. The path dependency of the sensitivity equation is identified and discussed. An accurate and efficient design sensitivity information is obtained with respect to die shape design parameters. The design optimization problem is solved to minimize the difference between the shape of the stamped workpiece after spring-back and the desired shape.

It is highly desired for design engineers to be able to simulate more complicated three-dimensional geometry for new developments in manufacturing processes. The effort to prevent wrinkling that appears frequently around the corner of the workpiece is a very important task in the stamping process. The proposed method can be extended to reduce wrinkling through the minimization of the difference between the stamped workpiece and the original desired shape. A three-dimensional contact algorithm and design sensitivity formulation will be developed in the near future for practical manufacturing problems.

ACKNOWLEDGEMENTS

This research was supported by the NSF/DARPA OPAAL (DMS 98-74015) and Ford University Research Program (URP 97-723R). This support is gratefully acknowledged.

REFERENCES

1. Haug EJ, Choi KK, Komkov V. *Design Sensitivity Analysis of Structural Systems*. Academic Press: New York, NY, 1986.
2. Zienkiewicz OC, Jain PC, Onate E. Flow of solids during forming and extrusion. *International Journal of Solids and Structures* 1978; **14**:15–38.
3. Maniatty AM, Chen MF. Shape sensitivity analysis for steady metal-forming processes. *International Journal for Numerical Methods in Engineering* 1996; **39**:1199–1217.
4. Antunez HJ, Kleiber M. Sensitivity of forming processes to shape parameters. *Computer Methods in Applied Mechanics and Engineering* 1996; **137**:189–206.
5. Zhao GQ, Wright E, Grandhi RV. Preform die shape design in metal forming using an optimization method. *International Journal for Numerical Methods in Engineering* 1997; **40**:1213–1230.
6. Chung SH, Hwang SM. Optimal process design in non-isothermal, non-steady metal forming by the finite element method. *International Journal for Numerical Methods in Engineering* 1998; **42**:1343–1390.
7. Balagangadhar D, Tortorelli DA. Design and analysis of large deformation continuous elastoplastic manufacturing processes via a steady displacement-based formulation. *7th AIAA/USAF/NASA/ISSMO Symposium on Multidisciplinary Analysis and Optimization*, St. Louise, MO, 1998; 1396–1406.
8. Lee EH. Elastic–plastic deformation at finite strains. *Journal of Applied Mechanics* 1969; **36**:1–6.

9. Simo JC. Algorithms for static and dynamic multiplicative plasticity that preserve the classical returs mapping schemes of the infinitesimal theory. *Computer Methods in Applied Mechanics and Engineering* 1992; **99**:61–112.
10. Moran B, Ortiz M, Shih CF. Formulation of implicit finite element methods for multiplicative finite deformation plasticity. *International Journal for Numerical Methods in Engineering* 1990; **29**:483–514.
11. Eterovic AL, Bathe KJ. A hyperelastic-based large strain elastoplastic constitutive formulation with combined isotropic-kinematic hardening using the logarithmic stress and strain measures. *International Journal for Numerical Methods in Engineering* 1990; **30**:1099–1114.
12. Weber G, Anand L. Finite deformation constitutive equations and a time integration procedure for isotropic, hyperelastic-viscoplastic solids. *Computer Methods in Applied Mechanics and Engineering* 1990; **79**:173–202.
13. Miehe C, Stein E, Wagner W. Associative multiplicative elastoplasticity: formulation and aspects of the numerical implementation including stability analysis. *Computers and Structures* 1994; **52**:969–978.
14. Badrinarayanan S, Zabaras N. A sensitivity analysis for the optimal design of metal-forming processes. *Computer Methods in Applied Mechanics and Engineering* 1996; **129**:319–348.
15. Wiechmann W, Barthold FJ. Remarks on variational design sensitivity analysis of structures with large elastoplastic deformations. *7th AIAA/USAF/ NASA/ISSMO Symposium on Multidisciplinary Analysis and Optimization*, St. Louise, MO, 1998; 349–358.
16. Sokolowski J, Zolesio JP. *Introduction to Shape Optimization*. Springer: Berlin, 1991.
17. Choi KK, Kim NH, Park YH. Shape design sensitivity analysis for contact problem with friction. *7th AIAA/USAF/NASA/ISSMO Symposium on Multidisciplinary Analysis and Optimization*, St. Louise, MO, 1998; 1071–1081.
18. Choi KK, Kim NH, Chen JS. Shape design sensitivity formulation for finite deformation elasto–plasticity with contact. *3rd World Congress of Structural and Multidisciplinary Optimization*, May 17–21, Buffalo, NY, 1999.
19. Hibbitt HD. Some follower forces and load stiffness. *International Journal for Numerical Methods in Engineering* 1979; **14**:937–941.
20. Schweizerhof K, Ramm E. Displacement dependent pressure loads in non-linear finite element analysis. *Computers and Structures* 1984; **18**:1099–1114.
21. Simo JC, Taylor RL, Wriggers P. A note on finite-element implementation of pressure boundary loading. *Communications in Applied Numerical Methods* 1991; **7**:513–525.
22. Belytschko T, Lu YY, Gu L. Element free Galerkin method. *International Journal for Numerical Methods in Engineering* 1994; **37**:229–256.
23. Belytschko T, Kronggauz Y, Organ D, Fleming M. Meshless methods: an overview and recent developments. *Computer Methods in Applied Mechanics and Engineering* 1996; **139**:3–47.
24. Liu WK, Jun S, Zhang YF. Reproducing kernel particle methods. *International Journal for Numerical Methods in Fluids* 1995; **20**:1081–1106.
25. Chen JS, Pan C, Wu CT, Liu WK. Reproducing kernel particle methods for large deformation analysis of non-linear structures. *Computer Methods in Applied Mechanics and Engineering* 1996; **139**:195–227.
26. Chen JS, Pan C, Roque CMDL, Wang HP. A Lagrangian reproducing kernel particle method for metal forming analysis. *Computational Mechanics* 1998; **22**:289–307.
27. Kim NH, Choi KK, Chen JS. Shape design sensitivity analysis and optimization of elasto–plasticity with frictional contact. *AIAA Journal* 2000; **38**:1742–1753.
28. Chen JS, Wang HP. New boundary condition treatments for meshless computation of contact problems, in press. *Computer Methods in Applied Mechanics and Engineering* 2000; **187**:441–468.
29. Chen JS, Yoon S, Wang HP, Liu WK. An improved reproducing kernel particle method for nearly incompressible finite elasticity. *Computer Methods in Applied Mechanics and Engineering* 2000; **181**:117–145.
30. Vanderplaats GM. *DOT user's manual*. VMA Corp.: Colorado Springs, CO, 1997.

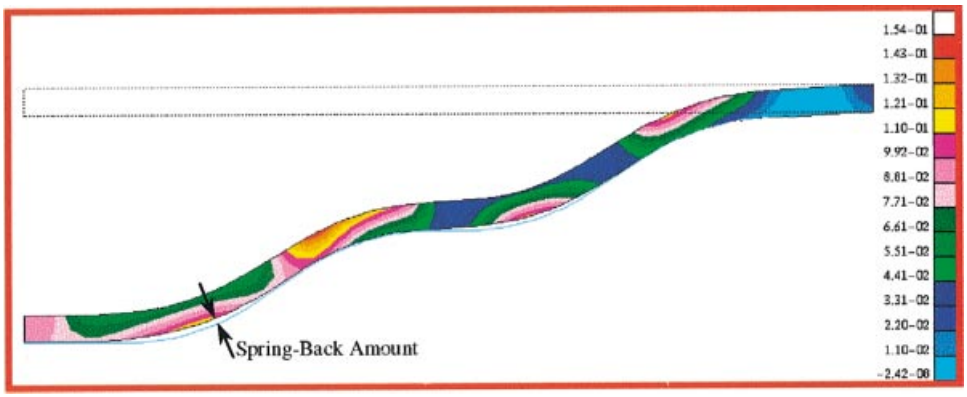

Plate 1. Contour plot of effective plastic strain.

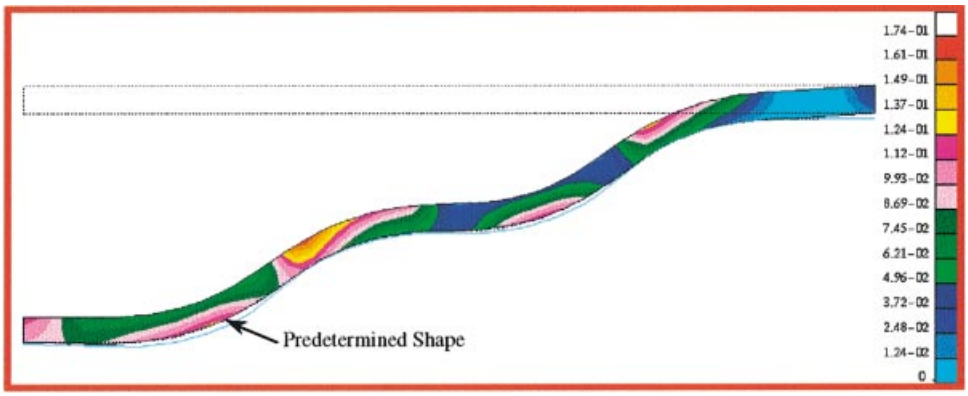

Plate 2. Optimized results of the effective plastic strain.